Opto-Electronic Advances

Original Article

2019, Vol. 2, No. 5

DOI: 10.29026/oea.2019.180028

Ultra-low cost Ti powder for selective laser melting additive manufacturing and superior mechanical properties associated

Yuhang Hou[1], Bin Liu[2], Yong Liu[2], Yinghao Zhou[1], Tingting Song[3], Qi Zhou[4], Gang Sha[4] and Ming Yan[1*]

One of the bottleneck issues for commercial scale-up of Ti additive manufacturing lies in high cost of raw material, i.e. the spherical Ti powder that is often made by gas atomization. In this study, we address this significant issue by way of powder modification & ball milling processing, which shows that it is possible to produce printable Ti powders based on ultra-low cost, originally unprintable hydrogenation-dehydrogenation (HDH) Ti powder. It is also presented that the as-printed Ti using the modified powder exhibits outstanding mechanical properties, showing a combination of excellent fracture strength (~895 MPa) and high ductility (~19.0% elongation).

Keywords: selective laser melting; powder modification; hydrogenation-dehydrogenation (HDH) Ti; ball milling; additive manufacturing

Hou Y H, Liu B, Liu Y, Zhou Y H, Song T T, Zhou Q *et al*. Ultra-low cost Ti powder for selective laser melting additive manufacturing and superior mechanical properties associated. *Opto-Electron Adv* **2**, 180028 (2019).

Introduction

Titanium and titanium alloys are widely used in aerospace, biomedical treatment, offshore drilling and many other industries, for their high specific strength, good corrosion resistance and excellent biocompatibility[1–3]. Additive manufacturing (AM), or 3D printing, has demonstrated its potent processing capability to realize near net shaping and/or customization particularly for parts of complex geometry, and therefore is becoming increasingly important[4,5]. Among the various AM approaches, selective laser melting (SLM) is one of the mostly investigated for exploring the opportunities for materials Ti and Ti alloys[6–10] in particular.

The cost of raw materials for SLM, i.e. the spherical Ti powders of good flowability, however, has long been a bottleneck issue to the scale-up of the technique[11]. The high cost is caused by at least two factors[12,13]: 1) The high-purity Ti ingot is not cheap itself, and 2) commercially-available powder production techniques, such as electrode induction-heating gas atomization (EIGA) and rotating electrode process (REP), require heavy equipment investment and costly processing consumables to use (e.g. high-purity Ar atmosphere), all pushing up the total cost on the spherical Ti powder. To the knowledge of the authors, the price of gas-atomized Ti powder is often around US$400 per kg. This is far more expensive than the hydrogenation–dehydrogenation (HDH) Ti powders[11]. The latter is around US$30 per kg. It is widely used in conventional powder metallurgy of Ti and Ti alloys but its morphology is highly irregular. It cannot be directly used for SLM because of its poor flowability.

On the other hand, if one can somehow modify the HDH-Ti powder to enable them to become printable by SLM, it may significantly open up the market for AM Ti and is therefore a pivotal research direction. In this regard,

[1]Department of Materials Science and Engineering, and Shenzhen Key Laboratory for Additive Manufacturing of High-performance Materials, Southern University of Science and Technology, Shenzhen 518055, China; [2]The State Key Laboratory of Powder Metallurgy, Central South University, Changsha 410083, China; [3]School of Aerospace, Mechanical and Manufacturing Engineering, Centre for Additive Manufacturing, RMIT University, Melbourne, VIC 3001, Australia; [4]School of Materials Science and Engineering, Nanjing University of Science and Technology, Nanjing 210094, China.

*Correspondence: M Yan, E-mail: yanm@sustc.edu.cn

Received 8 December 2018; accepted 30 January 2019; accepted article preview online 14 May 2019

ball milling & mechanical alloying (MA) can be a possible solution. It is well known that ball milling can be used to modify the morphology of metal powders[14–16]. Its capability to change the irregularly-shaped HDH-Ti powder into printable Ti powder, however, is yet to discover.

In this study, the ball milling technology was used to modify the HDH-Ti powder in an attempt to produce cost-affordable, printable Ti powders for SLM. The various process parameters, e.g. ball-to-material ratio, rotation speed and processing time, were systematically investigated. It will be shown that our efforts have finally led to encouraging results, demonstrating that it is possible to make the HDH-Ti powder printable and, simultaneously, the as-printed Ti shows fracture strength of ~ 895 MPa and elongation of ~19.0%. The underlying mechanism responsible for the mechanical performance is discussed using currently available alloy strengthening theories.

Experimental

HDH-Ti powder (average particle size: 35 μm, supplied by Central South University) was used in the powder modification. Gas atomized, spherical Ti powder (particle size: 15–45 μm) was purchased from the AP&C company (Canada) for comparative study.

Particle sizes of the modified powders were examined using a laser particle size analyzer (Mastersizer 3000, Worcestershire, United Kingdom). Powder flowability was studied by a comprehensive powder characteristics tester (PowderPro M1, BETTER, China). Flowability score like the ones shown in Table 1 can be given by the facility based on measurement of angle of repose, tap density, etc. Higher scores correspond to better flowability. Chemical composition of the powders was measured using inductively coupled plasma-atomic emission spectrometry (ICP-AES, Horiba Jobinyvon JY2000-2) as well as an O/N analyzer (LECO-ON736). Results were averaged based on at least three measurements.

For powder modification, a ball milling machine (Pulverisette5, Germany) was used and mill balls were made of 316 stainless steel. The ball milling processing was conducted under high-purity argon atmosphere.

The modified HDH-Ti powders were additively manufactured by an SLM machine (SLM 125HL, equipped with a 400 W IPG fiber laser) under high-purity Ar atmosphere. The as-purchased spherical Ti powder was printed as well for a comparative study. During the SLM process, the experimental variable was laser power (P= 110–140 W). Other parameters were as follows: 64 μm as laser beam diameter, 400 mm/s as scanning speed v, 0.030 mm as layer thickness l and 0.12 mm as hatch distance h.

Density of the as-printed samples was measured by the Archimedes method, and it was an averaged value based on three-time measurement of each sample. Relative density was calculated using 4.5 g/cm^3 as the theoretical density for the pure titanium. Tensile test was carried out using an Instron 3382 machine, equipped with a 10 mm extensometer and under a stretching rate of 0.2 mm/s on samples of 22 mm long, 3 mm thick and 4 mm wide. Hardness (HB) measurement was conducted on the THV-50MDX tester, where force was 0.1 kN and holding time was 10 s. Averaged values based on at least five measurements were used as the reported hardness, see Table 2.

Scanning electron microscopy (SEM, Zeiss Merlin, operated at 5 kV) and X-ray diffraction (XRD, Rigaku Smartlab, operated at 45 kV and 200 mA) with Cu Kα radiation were used for microstructural characterization, where the as-printed samples were etched with a solution consisting of HF (5 vol.%), HNO_3 (10 vol.%) and distilled water (85 vol.%). Transmission electron microscopy (TEM, Tecnai F30, operated at 300 kV) was used to detail the phases in the microstructure, where the samples were prepared by precision ion polishing system (PIPS). Atom probe tomography (APT, LEAP 4000X Si) was employed to examine atomic-level information, where samples were prepared using dual-beam Zeiss Auriga SEM/FIB with operating voltage up to 30 kV.

Table 1 | Particle size distribution, D50 and flowability score modified with different parameters. Parameter set No. D (underlined) shows the best combination of flowability and D50 values.

No.	Rotation speed (rpm)	Ball to materialal ratio	Process time (h)	D50 (μm)	Flowability score
Unmodified	-	-	-	35	74.5
A	80	5:1	2	42	78.1
B	80	10:1	2	28	75.6
C	100	5:1	2	73	85.3
D	**100**	**10:1**	**2**	**56**	**83.5**
E	100	15:1	2	126	86.1
F	100	10:1	4	246	90.7
G	120	5:1	2	87	84.2
H	120	10:1	2	76	83.8
I	150	5:1	2	189	88.6
J	150	10:1	2	106	85.1
K	200	5:1	2	59	74.2
L	200	10:1	2	48	72.8

Table 2 | Mechanical properties of the as-printed CP-Ti modified powder and the unmodified, spherical Ti powder. Different laser powers were used for printing the modified Ti powder, denoted as A-D.

Material type	Laser power (W)	Hardness (HB)	Young's modulus (GPa)	Tensile strength (MPa)	Ductility (%)
Unmodified CP-Ti	110	214	94.9	695	16.25
Modified CP-Ti (A)	110	242	104.3	820	14.94
Modified CP-Ti (B)	120	249	106.6	895	18.99
Modified CP-Ti (C)	130	252	100.1	770	19.40
Modified CP-Ti (D)	140	246	101.3	860	15.93

Results

Powder modification

Systematic powder modification experiments by ball milling were conducted to investigate the optimal processing parameters, via changing the ball-to-material ratio (5:1 or 10:1), the rotation speed (from 80 rpm to 200 rpm), and the processing time (2 h or 4 h). Figs. 1(a)–1(l) show the detailed powder modification results in terms of powder morphology. The information regarding the powder morphology, particle size variation (i.e. D50) and flowability were listed in Table 1. It is noted from the figure as well as the table that the ball milling parameters have significant impacts on the powder's flowability and particle size distribution. From the SLM processing perspective, the powders with high followability scores are preferred. Aside from this, powders with moderate particle sizes are desirable. For the most SLM facilities, powders of ~30–50 μm particle size are often used for achieving good geometry accuracy and surface quality. Smaller than this or too large powders may lead to flowability issue (for the former case) or poorer porosity (for the latter case).

To summarize the powder modification results, we list the following key findings. The relevant contents are further presented in Fig. 2 and Fig. 3:

1) After extensive experimental efforts, powder modification via ball milling has finally successfully changed the morphology of the HDH-Ti from highly irregular (Fig. 2(a)) to near spherical (Fig. 2(b)), using parameters of, e.g., 10:1 as the ball-to-material ratio, 100 rpm as the rotation speed and 2 h as the milling time, with an extra 0.2 wt.% steric acid as particle control agent (PCA), Fig. 1(d). Because of the much improved sphericalicity and enhanced flowability (Table 1 and Table 3), the modified powder can be well printed using SLM (Fig. 2(d)), which is in significant contrast to the unmodified HDH-Ti

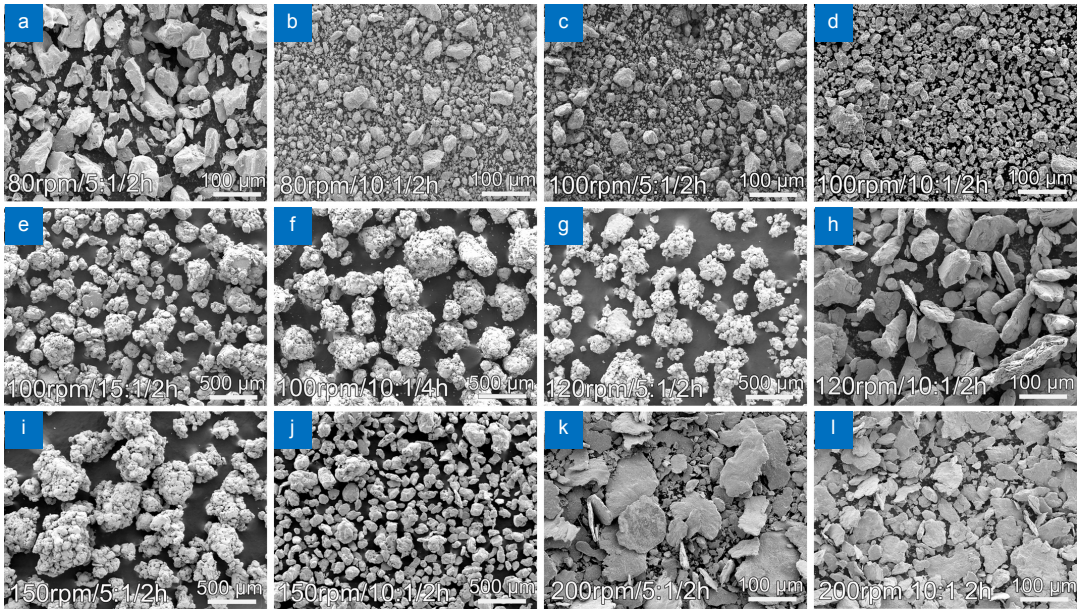

Fig. 1 | SEM images of the various HDH-Ti powders modified by the ball milling processing using different parameters.

Table 3 | Powder flowability results of the modified and unmodified HDH Ti powders.

Powder	Angle of repose (°)	Flat corner (°)	Crash angle (°)	Tap density (g/cm^3)	Overall score
HDH-Ti	38.66	61.00	27.00	2.38	74.5
Modified	33.00	37.33	20.66	2.48	83.5

powder (Fig. 2(c)). The latter fails to get well spread onto the substrate, or get detected by the powder-feeding sensor, then cannot be printed as a result.

2) After the powder modification, the powder has increased a bit in its particle size, from its original size of ~34.9 μm (D50) to ~56.9 μm (D50) as shown in Fig. 2(e). It is noted that the change has not affected the phase constitution of the powder, which shows the α′/α as the primary crystalline phase in the microstructure in Fig. 2(f). It is also noted that, after the powder modification, larger particles broaden the size distribution profile (Fig. 2(e)). One can always choose to add a sieving procedure to remove those larger particles and keep the smaller ones (e.g. 15–53 μm) for the subsequent 3D printing.

3) It is found that PCA is essential to the powder modification (see Fig. 3). The PCA used for this study is steric acid whose chemical formula is $CH_3(CH_2)_{16}COOH$. Without PCA, the powders tend to overwhelmingly aggregate (Fig. 3(a)) due to high surface energy of fresh Ti powder surface, once after the original surface oxide film (normally as TiO_2) on top of the Ti powder gets broken and removed during the ball milling process. Too much PCA, however, is deteriorative, for there will be almost no bonding between powder particles anymore and the morphology tends to become large flakes as shown in Fig. 3(b). With appropriate PCA (Fig. 3(c)), the milling processing only slightly increases the particle size, where the main function of PCA is to reduce surface energy of the powders, avoid their extraordinary aggregation (Fig. 3(d)), as well as reduce their adhesion to mill balls and internal area of the milling jar. It is noted that the melting and boiling temperatures of the steric acid are ~70 ℃ and ~360 ℃[17], respectively, suggesting that it may mostly remain in liquid state during the ball milling process but will vaporize during SLM[18]. From this perspective, too much PCA should also be avoided. Otherwise they may induce extra porosity to the as-printed microstructure. The residual of the steric acid may have contributed to the slight increase in O and C in the modified powder as well as in the as-printed Ti using the modified powder in Table 4.

4) The powder modification process has slightly changed the chemical composition of the HDH-Ti powder when compared before and after the ball milling (Table 4). Concentrations of O, N and Fe have slightly increased, which is most likely due to contamination pickup during ball milling including from the steel mill balls, and/or from the PCA.

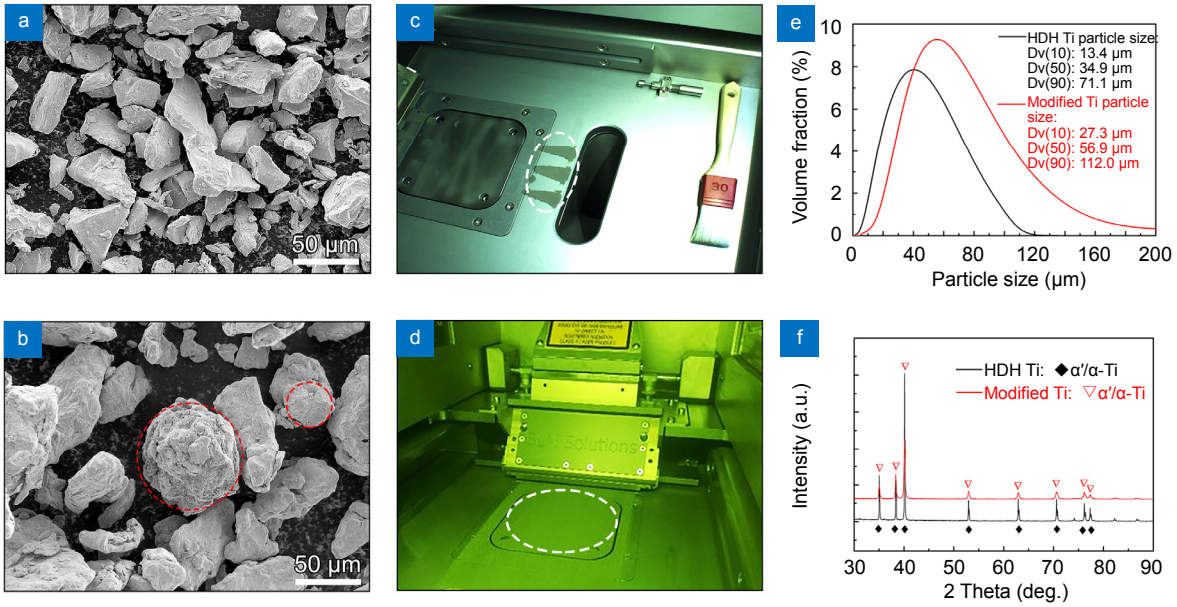

Fig. 2 | (**a**) SEM-SE image of unmodified HDH-Ti powder. (**b**) SEM-SE image of the modified HDH-Ti powder which shows near spherical morphology. (**c**) The powder spread record for the unmodified HDH-Ti powder (fails to spread onto substrate). (**d**) The powder spread record for the modified HDH-Ti powder (which is printable). (**e**) Particle size distribution before and after powder modification. (**f**) XRD results for the powders before and after powder modification.

Table 4 | Chemical compositions of the unmodified and modified HDH-Ti powder, and the as-printed Ti using the modified HDH-Ti and as-purchased spherical Ti powder.

	Mo (wt.%)	Cr (wt.%)	Ni (wt.%)	Mn (wt.%)	Fe (wt.%)	C (wt.%)	N (wt.%)	O (wt.%)
HDH-Ti	< 0.05	< 0.05	< 0.05	< 0.05	< 0.05	0.032	0.0069	0.218
Modified	< 0.05	0.019	0.028	< 0.05	0.07	0.044	0.0126	0.273
As-printed Ti	< 0.05	0.013	0.026	< 0.05	0.05	0.071	0.0130	0.330
Spherical Ti	-	-	-	-	0.02	0.020	0.020	0.150

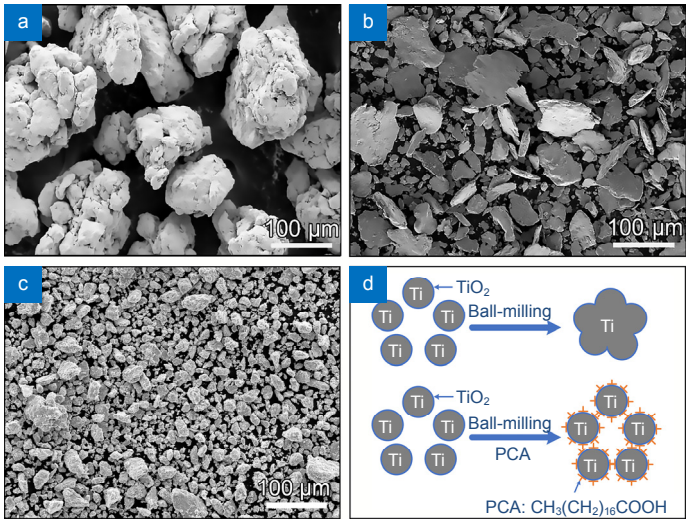

Fig. 3 | Powder morphology variation using different amount of PCA, (a) 0 wt.%, (b) 1 wt.% and (c) 0.2 wt.%, and (d) schematic graph to show the effect of PCA on the powder modification. The original TiO_2 film on top of powder surface may get resolved into Ti matrix during SLM process.

Microstructure and mechanical property of the as-printed Ti

The modified HDH-Ti powder was subsequently additively manufactured by SLM. The microstructure of the as-printed Ti was revealed by XRD, SEM, TEM and APT. Typical XRD results are shown in Fig. 4(a), which show overwhelmingly needle or lath shaped martensitic Ti (α′, hcp structured with a=0.294 nm and c=0.467 nm[19]) in the microstructure. The corresponding SEM secondary electron (SEM-SE) image in Fig. 4(b), TEM bright field (TEM-BF) image in the figure inset and EBSD results (Figs. 4(c) and 4(d)) all confirm this. Such microstructure is typical to SLMed CP-Ti. One difference between the as-printed microstructures using modified and spherical powder is that the former shows slightly finer grain size (~20 μm long and ~6 μm wide), see Figs. 4(c) and 4(d). During the ball milling powder modification procedure, extra chances for impurity elements pickup and large internal residual stress likely lead to more heterogeneous nucleation centers (due to the former factor) and fragmentation/refinement (due to the latter factor), contributing to the observation[14–16].

Fig. 4(e) shows the engineering tensile stress–strain curves using different SLM parameters. The best mechanical properties (i.e. ~895 MPa as the fracture strength and ~19.0% as the elongation) are achieved at 120 W laser power and 400 mm/s scanning speed, whose corresponding energy density ($=P/(v{\cdot}l{\cdot}h)$) is 83.3 J/mm^3. The SEM-SE image shows the fractography of the as-printed sample, demonstrating a large amount of ductile, dimple-like deformation units, Fig. 4(f). This is consistent with the excellent ductility measured, although cleavage fracture areas are also observable in the fractography. It needs to be mentioned that there are few inclusions like the one in the bottom right in Fig. 4(f). They are most likely residuals of the steel mill balls, which are ground off during the ball milling procedure.

APT was further employed to detail the microstructure at the atomic level. Fig. 4(g) shows the analyzed volume (within a box of ~85 nm× 85 nm× 286 nm) of a tip APT sample. One small oxygen (O) rich region of nanometer scale is observed in the upper left corner of the analyzed volume refined by an isosurface of 6 at.%O (Fig. 4(h)). The rest of the tip sample shows homogenous and dilute distribution of oxygen. 1D concentration profiles of O and Fe measured along the marked direction in Fig. 4(g) are shown in Fig. 4(i), also confirming that the particle is relatively rich in oxygen and slightly poor in Fe compared to the matrix.

Oxygen is α-Ti stabilizer, while Fe is a well-known β-Ti stabilizer[1–3]. A quick reference to the Ti-Fe phase diagram[20] suggests a schematic graph like the Fig. 4(j). It shows that the β-Ti→α-Ti+TiFe reaction is possible at equilibrium condition, but in reality the reaction is sluggish and hardly happens[21], particularly in the case of SLM whose cooling rate can be even higher than 10^4 K/s[4,5]. The matrix shown in Fig. 4(g) is therefore α′ phase originating from martensite phase transformation during cooling from high temperature and the phase should be resulted from the parent β-Ti phase, which chemical concentration is relatively rich in Fe. The oxygen-enriched nanoparticle shown in Fig. 4(g) is likely to be α-Ti (hcp structured with a=0.292 nm and c=0.466 nm[19]), which is resulted from decomposition of α′ phase caused by surrounding heat source. Since the lattice parameters of the α-Ti phase are slightly smaller than those of the α′, existence of these α-Ti phases will lead to a right shift of XRD pattern to the higher 2θ direction. The two XRD peaks, however, also overlap a bit to each other, making it difficult to differentiate unambiguously in Fig. 4(a).

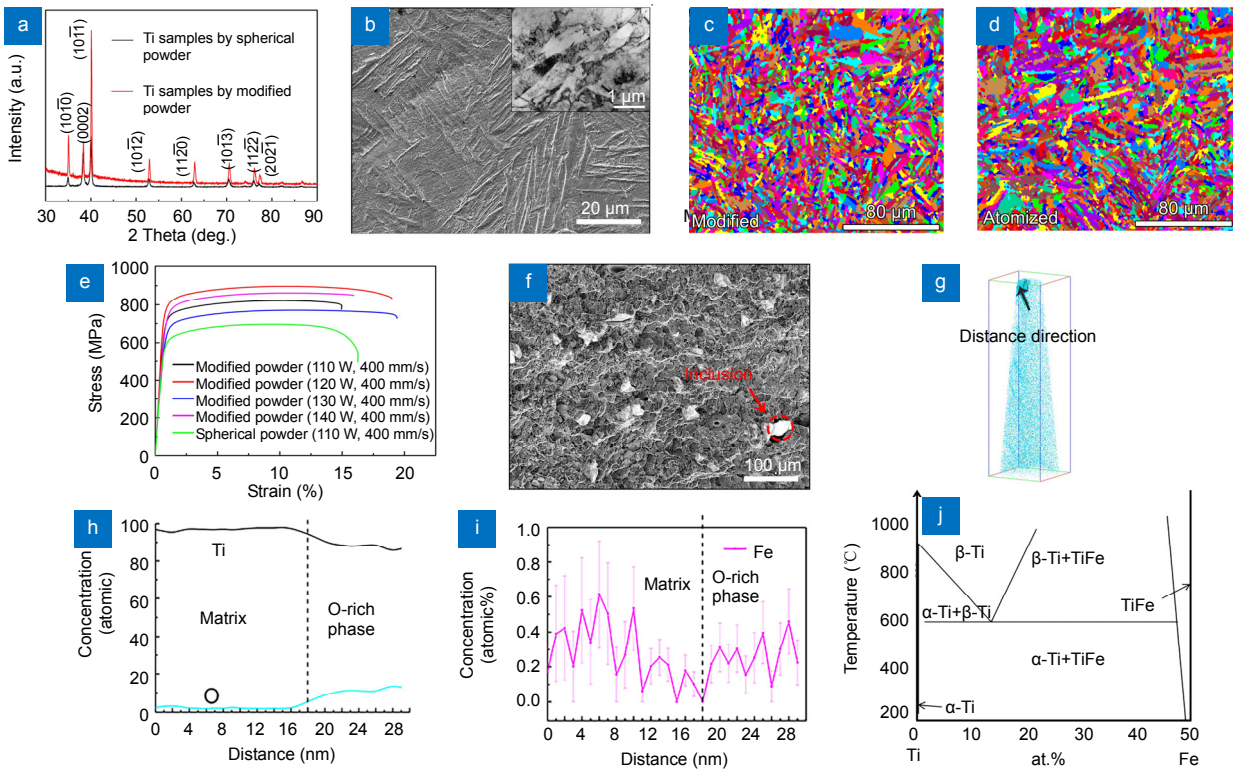

Fig. 4 | (**a**) XRD patterns for the as-printed Ti using modified powder and spherical powder. (**b**) SEM-SE image of the as-printed Ti using the modified powder; figure inset is a TEM-BF image. (**c**) EBSD result for the modified CP-Ti powder. (**d**) EBSD result for the as-purchased CP-Ti powder. (**e**) Tensile test of the as-printed Ti using the modified powder, with a comparative curve based on the commercial spherical Ti powder. (**f**) Fractography of the as-printed Ti using the modified powder, where inclusion can be occasionally found as the one marked out. (**g**) 3D APT results showing the oxygen distribution across the tip sample. (**h**) and (**i**) The corresponding concentration profiles of oxygen and Fe, and (**j**) schematic graph of part of a Ti-Fe binary phase diagram.

Discussion

Through above study, we have demonstrated that, by way of powder modification, one can: (a) produce ultra-low cost CP-Ti powders for SLM and, equally importantly, and (b) realize excellent mechanical properties by the as-printed samples using the modified powder. The two points are discussed as follows.

Discussion and comments on the powder modification approach

Regarding the point (a), for a successful powder modification, one may have to consider the following factors:

1) The flowability and particle size of the modified powders should be acceptable. Our results shown in Fig. 2 and Fig. 3 as well as in Table 1 and Table 3 illustrate that the modified powder shows excellent printability after the powder modification by ball milling. The slightly increased particle size turns out to be fine from densification perspective, which leads to an as-printed relative density of 98.89% when using the same SLM parameters as for the as-purchased, spherical CP-Ti powder.

2) The chemical composition before and after the powder modification should be within the permissible range. The as-purchased HDH Ti belongs to the Grade 2 CP-Ti from oxygen concentration perspective. Our results show that after the powder modification, the oxygen concentration raises from 0.218 wt.% to 0.272 wt.%. The value falls within the range of the Grade 3 CP-Ti, which permits a maximum of 0.35 wt.% oxygen. Other major alloying/interstitial elements such as Fe and C are also within the allowed range of Grade 3 CP-Ti. These findings suggest that the modified CP-Ti can be used in the circumstances where the Grade 3 CP-Ti applies.

3) The phase constitution of the modified powder should be close to that of the as-supplied powder. This has been confirmed by the XRD results shown in Fig. 2(f).

4) Lastly, the modified powder should have significant cost advantage. Regarding this, we claim that the cost of raw material, i.e. the printable Ti powder, can be significantly reduced using our approach. This is demonstrated well by Fig. 5(a), which highlights the cost difference between the modified HDH-Ti powder and the commercially available, spherical Ti powder, along with other Ti materials[11]. It should be mentioned that the price for the modified HDH-Ti powder has not incorporated the extra cost relating to the ball milling processing adopted in the study. Nevertheless, the difference is huge, showing that the modified powder is merely ~1/10 of the commercial, spherical powder in terms of cost.

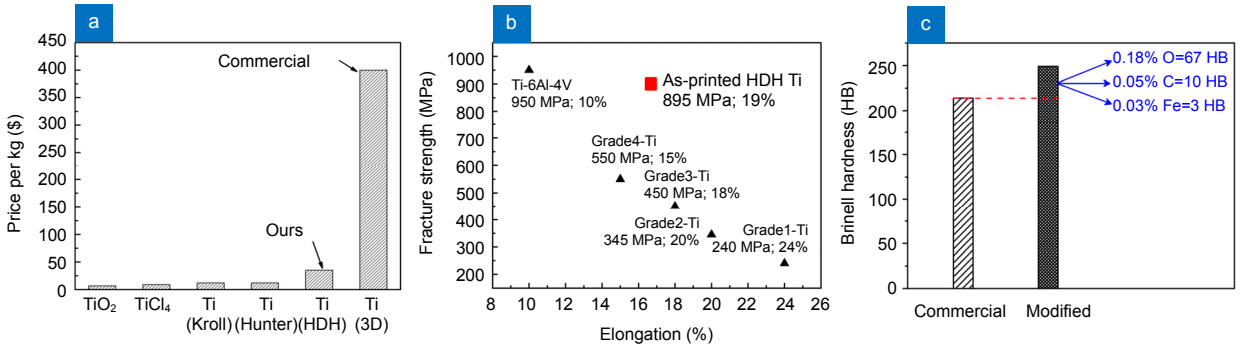

Fig. 5 | (**a**) Comparison of the prices of a variety of Ti materials highlighting the ultralow cost Ti powder developed in this study. (**b**) Comparison of the mechanical properties among some typical Ti materials. (**c**) The Brinell hardness of the as-printed CP-Ti using commercial, spherical powder and modified powder; the latter shows better hardness due to enlarged concentration of N, O and Fe.

Discussion on the mechanical property of the as-printed Ti

Regarding the point (b), the as-printed Ti using the modified powder has shown excellent mechanical properties compared with the other Ti materials, including the Grade 1– Grade 4 CP-Ti and Ti-6Al-4V[1,2,22]. One can note that the as-printed Ti developed by this study has excellent strength (~895 MPa) as well as high ductility (~19.0%). This makes it be far better than the conventional CP-Ti materials in terms of strength and even superior to Ti-6Al-4V in terms of fracture toughness, Fig. 5(b).

The contributions to the mechanical properties achieved can be discussed as follows:

1) Interstitial element strengthening effects from the ball milling and the SLM processing should be the dominant contributing factor. Table 4 lists concentrations of the interstitial N, O, and C elements. It is well known that N and O are beneficial to the strength/hardness of CP-Ti by the solid solution strengthening mechanism[23]. It has been proposed that the overall hardness of Ti can be estimated by following the relationship: Brinell hardness $= 196\sqrt{\%N} + 158\sqrt{\%O} + 45\sqrt{\%C} + 20\sqrt{\%Fe} + 57$ [24,25]. Table 2 shows that, compared with the spherical Ti, the as-printed CP-Ti using modified powder has increased hardness from ~214 HB to ~249 HB. Meanwhile, increments of 0.18 wt.%O and 0.05 wt.%C may contribute to enlarged hardness up to 67 HB and 10 HB, respectively, according to the above model (see Fig. 5(c)). Nevertheless, these suggest that the O and N dissolved should be the most influential factor to the excellent mechanical performance realized by the as-printed CP-Ti using the modified powder.

2) Meanwhile, the slight increase in Fe in the modified powder (Table 4) may also have contributed to the overall hardness/strength according to the aforementioned analysis.

3) The residual α-Ti nanoparticles existing in the matrix (see Fig. 4(g)) may have led to better ductility than a pure martensitic microstructure, as α-Ti is a ductile phase itself.

4) Grain refinement factor due to rapid cooling associated with SLM[4,5], which contributes to both strength and ductility of the as-printed Ti, when compared with the conventionally made CP-Ti materials. This also explains why the as-printed Ti using the as-purchased powder shows better overall mechanical properties than the conventional Grade 1- Grade 4 CP-Ti in Fig. 5(b).

Conclusions

In this study, we have offered a powder modification approach, which is able to provide ultra-low cost, printable Ti powders for SLM by manipulating the irregularly-shaped, originally unprintable HDH-Ti powder. The impacts of the results are at least twofold and can be summarized as follows:

1) To solve the long-time bottleneck issue for Ti 3D printing that is the high cost on raw powder material. The present results show that the ball milling & mechanical alloying is capable to modify the unprintable HDH CP-Ti into printable CP-Ti powder, and the best parameters so far are 10:1 as the ball-to-material ratio, 100 rpm as the rotation speed and 2 h as the milling time. It is also revealed that the process control agent, PCA, is essential for successful powder modification.

2) To provide an as-printed CP-Ti material whose mechanical properties are excellent, showing its maximum facture strength (~895 MPa) close to that of Ti-6Al-4V but with even higher elongation (~19.0%). The corresponding relative density is 98.89%, which still has room to get further improved. We have clarified that slight pickup of O, N and Fe during the powder modification and the SLM processing has contributed to the excellent mechanical performance.

References

1. Leyens C, Peters M. *Titanium and Titanium Alloys*: *Fundamentals and Applications* (Wiley-VCH, Weinheim, 2003).
2. Lütjering G, Williams J C. *Titanium. Engineering Materials and Processes*, 2nd ed (Springer-Verlag, Berlin, 2007).

3. Yan M, Dargusch M S, Ebel T, Qian M. A transmission electron microscopy and three-dimensional atom probe study of the oxygen-induced fine microstructural features in as-sintered Ti–6Al–4V and their impacts on ductility. *Acta Mater* **68**, 196–206 (2014).
4. Lu B H, Lan H B, Liu H Z. Additive manufacturing frontier: 3D printing electronics. *Opto-Electron Adv* **1**, 170004 (2018).
5. Qian M, Xu W, Brandt M, Tang H P. Additive manufacturing and postprocessing of Ti-6Al-4V for superior mechanical properties. *MRS Bull* **41**, 775–784 (2016).
6. Thijs L, Verhaeghe F, Craeghs T, Van Humbeeck J, Kruth J P. A study of the microstructural evolution during selective laser melting of Ti-6Al-4V. *Acta Mater* **58**, 3303–3312 (2010).
7. Zhou Y H, Lin S F, Hou Y H, Wang D W, Zhou P *et al*. Layered surface structure of gas-atomized high Nb-containing TiAl powder and its impact on laser energy absorption for selective laser melting. *Appl Surf Sci* **441**, 210–217 (2018).
8. Qiu C L, Adkins N J E, Attallah M M. Microstructure and tensile properties of selectively laser-melted and of HIPed laser-melted Ti-6Al-4V. *Mater Sci Eng*: *A* **578**, 230–239 (2013).
9. Ouyang D, Li N, Xing W, Zhang J J, Liu L. 3D printing of crack-free high strength Zr-based bulk metallic glass composite by selective laser melting. *Intermetallics* **90**, 128–134 (2017).
10. Li N, Zhang J J, Xing W, Ouyang D, Liu L. 3D printing of Fe-based bulk metallic glass composites with combined high strength and fracture toughness. *Mater Des* **143**, 285–296 (2018).
11. Yan M, Yu P. An Overview of densification, microstructure and mechanical property of additively manufactured Ti-6Al-4V—Comparison among selective laser melting, electron beam melting, laser metal deposition and selective laser sintering, and with conventional powder. In Lakshmanan A, *Sintering Techniques of Materials* (IntechOpen, London, 2015).
12. Upadhyaya G S. *Powder Metallurgy Technology* (Cambridge International Science Publishing, Cambridge, 1998).
13. Lu S C. *Powder Technology Handbook* (Chemical Industry Press, Beijing, 2004).
14. Benjamin J S, Volin T E. The mechanism of mechanical alloying. *Metall Trans* **5**, 1929–1934 (1974).
15. Suryanarayana C. Mechanical alloying and milling. *Prog Mater Sci* **46**, 1–184 (2001).
16. Gilman P S, Benjamin J S. Mechanical alloying. *Ann Rev Mater Sci* **39**, 279–300 (1983).
17. Lide D R. *CRC Handbook of Chemistry and Physics*, *2009-2010* 90th ed (CRC Press, Boca Raton, 2009).
18. Xi S Q, Qu X Y, Zheng X L, Ma M L, Liu X K *et al*. *Mater Sci Tech* **5**, 45 (1997).
19. Yang J J, Yu H C, Yin J, Gao M, Wang Z M *et al*.Formation and control of martensite in Ti-6Al-4V alloy produced by selective laser melting. *Mater Des* **108**, 308–318 (2016).
20. Murray J L. Fe-Ti (Iron-Titanium). In Okamoto H, *Phase Diagrams of Binary Iron Alloys* (ASM International, Materials Park, OH, 429–432, 1993).
21. Yan M, Qian M, Song T T, Dargusch M S. Significant α-phase growth confinement in Grade 4 titanium and substantial *β*-phase refinement in Grade 7 titanium. *MRS Commun* **4**, 183–188 (2014).
22. ASTM B861-10, Standard Specification for Titanium and Titanium Alloy Seamless Pipe, (ASTM International, West Conshohocken, PA, 2010), www.astm.org.
23. Yan M, Xu W, Dargusch M S, Tang H P, Brandt M *et al*. Review of effect of oxygen on room temperature ductility of titanium and titanium alloys. *Powder Metall* **57**, 251–257 (2014).
24. Conrad H. Effect of interstitial solutes on the strength and ductility of titanium. *Prog Mater Sci* **26**, 123–403 (1981).
25. Luo S D, Li Q, Tian J, Wang C, Yan M *et al*. Self-assembled, aligned TiC nanoplatelet-reinforced titanium composites with outstanding compressive properties. *Scr Mater* **69**, 29–32 (2013).

Acknowledgements

This work was supported by Shenzhen Science and Technology Innovation Commission (No. ZDSYS201703031748354), and National Science Foundation of Guangdong Province (No. 2016A030313756). This work was also supported by the Pico Center at SUSTech with support from the Presidential fund and Development and Reform Commission of Shenzhen Municipality (No. 2016-726). Dr. M. Yan thanks support from the Humboldt Research Fellowship for Experienced Researchers.

Competing interests

The authors declare no competing financial interests.